Solar Energy Materials & Solar Cells 248 (2022) 111987

Contents lists available at ScienceDirect

Solar Energy Materials and Solar Cells

journal homepage: www.elsevier.com/locate/solmat

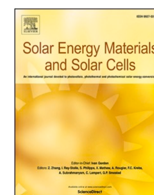

Optimized molecular beam epitaxy process for lattice-matched narrow-bandgap (0.8 eV) GaInNAsSb solar junctions

Riku Isoaho *, Antti Tukiainen, Juuso Puutio, Arttu Hietalahti, Jarno Reuna, Antti Fihlman, Elina Anttola, Miika Keränen, Arto Aho, Mircea Guina

Optoelectronics Research Centre, Physics Unit, Faculty of Engineering and Natural Sciences, Tampere University, P.O. Box 692, FI-33014, Tampere, Finland

ARTICLE INFO

Keywords:
Dilute nitrides
Molecular beam epitaxy
Growth parameters
GaInNAsSb
Multijunction solar cells

ABSTRACT

High performance narrow-bandgap GaInNAsSb solar cells are instrumental for the development of lattice-matched GaAs-based solar cells with more than four junctions. To this end a comprehensive optimization process including the effects of growth temperature, As/III beam equivalent pressure ratio, and Sb flux on the performance of 0.8 eV GaInNAsSb solar cells grown by molecular beam epitaxy is reported. For this, sets of GaInNAsSb p-i-n solar cell structures with 5–6% nitrogen compositions were fabricated, while varying the key growth parameters. The quantum efficiency and current generation increased significantly when the narrow gap materials were grown at elevated growth temperatures, close to phase separation. A further improvement in the current generation was observed by employing lower As/III beam equivalent pressure ratios. The best GaInNAsSb cell exhibited about 94% peak external quantum efficiency and generated a short-circuit current of 17.7 mA/cm^2 with AM1.5D (1000 W/m^2) illumination at wavelengths above 900 nm without employing a back surface reflector. Our analysis indicates that the best cell is already close to being absorption limited. While the N composition should be kept as low as possible (i.e., $\lesssim$5%) to achieve high performance, increasing the Sb flux generally results in improved the material quality, i.e., leading to a slight improvement for the open-circuit voltages and fill factors. In addition, it was found that the phase separation observed at the growth temperature of 480 °C could effectively be inhibited by employing higher Sb fluxes.

1. Introduction

Ultra-high conversion efficiencies can be achieved with multi-junction solar cells (MJSC) based on III–V materials using various approaches [1,2]. Currently, the world record efficiency of 47.6% has been set by a wafer-bonded four-junction (4J) solar cell [3], but high efficiencies up to 44% have also been demonstrated by lattice-matched (LM) solar cell devices comprising dilute nitride subcells [4–6]. In this particular LM approach, the germanium bottom junction commonly used for GaInP/GaInAs/Ge triple-junction (3J) cells [7], is replaced with dilute nitride GaInNAs(Sb) subcell with a more optimal bandgap energy (E_g) of ~1 eV [8], and typically the MJSC stack is grown on GaAs. The LM approach offers benefits in terms of processing and epitaxy since relatively standard post-growth processing can be utilized, and the epitaxy does not involve growth of thick passive buffer layers. The dilute nitride compounds, where a small fraction of other group-V atoms is replaced with N, are attractive for MJSC applications since they are the only III–V materials, with the exception of GaAsPBi [9], that can be grown lattice-matched to GaAs while reaching bandgaps down to 0.7 eV [5,10]. However, due to the limited solubility of N into III–V compounds at thermal equilibrium [11] and large miscibility gap [12], metastable dilute nitrides need to be grown at significantly lower temperatures than traditional III–V materials [13,14]. The optimal growth temperature range for dilute nitrides is limited by formation of various crystalline point defects at low temperatures [15,16] and by phase separation at high growth temperatures [17,18]. The formation of point defects and phase separation both have detrimental impact on the material quality and device operation. The adverse effects of N also get more pronounced with higher N concentrations [17–20]. In general, dilute nitride solar cells are infamous for suffering from short minority carrier lifetimes [21,22], short diffusion lengths [15] and high background doping densities [23], which have hindered their wide spread use for solar cells. However, the use of molecular beam epitaxy (MBE) has proven to be effective for growing high-quality 1 eV GaInNAs(Sb) materials with

* Corresponding author.
E-mail address: riku.isoaho@tuni.fi (R. Isoaho).

https://doi.org/10.1016/j.solmat.2022.111987
Received 3 June 2022; Received in revised form 29 July 2022; Accepted 2 September 2022
Available online 14 September 2022
0927-0248/© 2022 The Authors. Published by Elsevier B.V. This is an open access article under the CC BY license (http://creativecommons.org/licenses/by/4.0/).

approximately 3–4% N compositions, resulting in development of high performance LM MJSCs [5,24,25]. However, reaching the so far elusive 50% efficiency level would essentially require increasing the number of junctions to five or more [26,27]. For certain five-junction (5J) and six-junction (6J) MJSC designs it could be beneficial to employ a ~0.8 eV subcell as the bottom junction of the stack [28]. In the LM approach this would require development and use of new subcells and junction materials for the narrow bandgap region. A somewhat obvious solution for bridging the gap between the 1 eV GaInNAs(Sb) and germanium (0.67 eV) in the infrared spectral region would be to increase the N content of GaInNAs(Sb) alloy, but reaching bandgap energies of ~0.8 eV already requires approximately 6% N compositions. With this high N compositions the adverse effects associated with higher N incorporation make the successful fabrication of GaInNAs(Sb) junctions with quality necessary for MJSC integration challenging [29]. However, the unwanted effects of N can be drastically reduced by optimization of growth parameters [14,23,30], use of growth surfactants [31–33], and thermal annealing [15,34]. Recently, we have demonstrated thin GaInNAsSb single junction solar cells grown by MBE with 6–8% N concentrations corresponding to bandgap energies between 0.7 eV and 0.8 eV [35]. It was estimated that a lattice-matched 6J design with subcell bandgaps of 2.0–2.2 eV, 1.92 eV, 1.63 eV, 1.40 eV, 1.18 eV and 0.78 eV utilizing the demonstrated 0.78 eV GaInNAsSb subcell could already realistically attain efficiencies in the range of 50.4–52.1% at 1000 suns. Yet, despite demonstrating promising results for MJSC integration, there was significant room for improving the solar cell performance, especially in terms of current generation for achieving current-matched operation. By introducing a back surface reflector underneath the GaInNAsSb junction, higher current densities were obtained, yet further improvements would still be needed for practical deployment of the junction in a MJSC stack [36]. Here we have extended the optimization of the epitaxy process and studied the effects of growth temperature, arsenic overpressure, and Sb flux on the performance of MBE-grown narrow gap GaInNAsSb single junction solar cells in an effort of improving their performance.

2. Experimental

2.1. Growth and processing

Three sets of GaInNAsSb single junction p-i-n solar cells with varying growth temperatures (T_g), As/III beam equivalent pressure (BEP) ratios and Sb fluxes were grown on 4" p-GaAs(100) substrates using Veeco GEN20 plasma-assisted solid-source MBE system. The MBE system was equipped with SUMO cells for group-III elements, valved cracker sources for As and Sb, and a radio-frequency (RF) plasma source for atomic N. The grown heterostructures consisted of 1.2 μm thick unintentionally doped GaInNAsSb layer embedded between 100 nm of n-type and p-type GaAs, 100 nm p-$Al_{0.35}Ga_{0.65}As$ back surface field layer, 40 nm n-$Al_{0.35}Ga_{0.65}As$ window layer, and 300 nm of highly doped n-GaAs contact layer. The E_g of the GaInNAsSb layers was targeted at ~0.8 eV. The nominal In composition for the *i*-layers in the majority of the structures was 15%. The nominal N concentrations estimated using the plasma parameters [37] were around 5%, yet minor adjustments were made between growths in an effort to maintain the ~0.8 eV bandgap and sufficient lattice-matching. For the first set of samples (A–F) the growth temperature of the GaInNAsSb layer, measured with a thermocouple, was varied between 440 °C and 480 °C, while keeping the As/III BEP ratio at 9.0 and the BEP for Sb at ~1.0×10^{-8} Torr. Then, based on the first set of samples, structures (G–H) were grown at $T_g = 470$ °C with BEP of ~1.0×10^{-8} Torr for Sb, while the As/III BEP ratio was lowered to 7.0 and 5.2. For the next structures (I–J), the Sb flux was increased to ~1.4 $\times 10^{-8}$ Torr and ~1.8×10^{-8} Torr, while using $T_g = 470$ °C and As/III BEP ratio of 7.0. For samples grown with the highest Sb flux the In composition was reduced to ~14% in order to maintain better lattice-matching as higher Sb incorporation was expected. Finally, one additional structure (K) was grown with the higher Sb flux of ~1.8 $\times$ 10^{-8} Torr, but the T_g was raised to 480 °C. All the structures were selected to be *in-situ* annealed at 700 °C for 20 min under As overpressure of ~1×10^{-5} Torr. Modest ramp rate (20 °C/min) was used for the annealing step. The annealing was not part of the optimization for this work, and the optimum annealing parameters for these high-N materials are likely to be different from the used parameters. The differences in the growth parameters of the structures are compiled into Table 1.

The grown wafers were processed into 6 mm × 6 mm solar cells with an active area of 0.25 cm^2. The active area was used for determining the current density values of the experimental solar cells in the following sections. A double layer TiO_x/SiO_y (112 nm/178 nm) antireflection coating (ARC), designed for low reflectance in the near infrared region, was deposited on the devices using ion beam sputtering. The ARC was also deposited on separate reflectance sample pieces without front metal grids and a piece of blank n-GaAs substrate.

2.2. Material and device characterization

The optical and structural properties of the grown wafers were characterized by photoluminescence (PL) and x-ray diffraction (XRD) measurements. The room-temperature PL measurements were conducted with an Accent RPM2000 PL mapper using a Q-switched 1064 nm laser for excitation. For evaluating the lattice-matching and crystalline quality of the GaInNAsSb layers, ω-2θ scans around (004) reflection and reciprocal space maps (RSM) around symmetric (004) and asymmetric (-2-24) reflections were measured using a high-resolution Panalytical X'Pert[3] triple-axis XRD system equipped with a PIXcel3D detector.

The electrical performance of the solar cell devices was characterized by measuring dark current-voltage (dark-IV), light-biased current-voltage (LIV), and external quantum efficiency (EQE). The dark-IV and LIV measurements were made with an OAI TriSol 7 kW solar simulator at 25 °C. The LIV measurements were performed under simulated AM1.5D (1000 W/m^2 normalization) spectrum filtered with a 900 nm long-pass filter to emulate excitation in a MJSC stack. The EQE measurements were performed using a monochromator-based setup equipped with a 250 W quartz-tungsten halogen lamp and suitable edge-pass filters. The signal calibration for the EQE system was performed using NIST-calibrated (National Institute of Standards and Technology) Si and Ge reference detectors. In addition, the bandgap energies of the GaInNAsSb materials were estimated from the band edges of the measured EQEs. The specular reflectance spectra for the separate reflectance samples were measured at 8° incidence angle using a PerkinElmer Lambda 1050 spectrophotometer.

2.3. Modelling

The E_g values from the EQE measurements and the strain (ε_{xx})

Table 1
The nominal In and N compositions, growth temperatures, As/III BEP ratios, and Sb pressures for the grown GaInNAsSb solar cell structures.

Sample	$[In]_{nominal}$ (%)	$[N]_{nominal}$ (%)	T_g (°C)	As/III BEP ratio	Sb BEP (Torr)
A	15	5.2	440	9.0	1.0×10^{-8}
B	15	5.7	440	9.0	1.0×10^{-8}
C	15	5.2	450	9.0	1.0×10^{-8}
D	15	5.2	460	9.0	1.0×10^{-8}
E	15	5.0	470	9.0	1.0×10^{-8}
F	15	5.0	480	9.0	1.0×10^{-8}
G	15	5.0	470	7.0	1.0×10^{-8}
H	15	4.9	470	5.2	1.0×10^{-8}
I	15	4.8	470	7.0	1.4×10^{-8}
J	14	4.8	470	7.0	1.8×10^{-8}
K	14	4.8	480	7.0	1.8×10^{-8}

obtained from the XRD measurements were used for estimating the material compositions (In, N and Sb) for the GaInNAsSb layers by using an interpolation scheme based on band anti-crossing models [38].

For evaluating the carrier lifetimes and background doping levels in the GaInNAsSb materials, the experimental EQE and LIV characteristics were modelled with PC1D simulation software (v.5.9) [39]. By iteratively fitting the short-circuit current density (J_{sc}), open-circuit voltage (V_{oc}) and EQE given by the PC1D model with the experimentally determined values, estimates for the bulk carrier lifetime (τ) and carrier concentrations were obtained.

3. Results and discussion

3.1. Material characterization

The experimentally obtained E_g and ε_{xx} values for the GaInNAsSb materials are listed in Table 2. The strain in the GaInNAsSb is defined as $\varepsilon_{xx}=(a_{GaInNAsSb}-a_s)/a_s$, where $a_{GaInNAsSb}$ and a_s are the lattice constants of the dilute nitride layer and the GaAs substrate, respectively [40]. In addition, Table 2 includes the best-fit values for In, N and Sb compositions for the GaInNAsSb materials obtained through the modelling.

In general, the bandgap energies of GaInNAsSb materials were quite close to the targeted value of 0.8 eV with ~6% N compositions. But within the T_g set (A–F) there was slight variation in the N compositions and determined bandgaps. For structure F, grown at 480 °C, the material composition and E_g could not be determined as the GaInNAsSb material had phase separated, resulting in an inferior material quality. Compared to the rest of the structures with more than 6% of N, lower N composition of ~5% were determined for samples A and C, which translates into larger E_g values of these samples. For sample A the attained [N] was very close to the nominal value (Table 1), but the N concentration was simply too low for reaching the target E_g of 0.8 eV. Consequently, for the growth of structure B, the nominal N was increased. However, now the N composition did not follow the predicted value like for sample A. Instead, the attained N composition for sample B was observed to be 1.16 times higher than the target, indicating change in the incorporation kinetics of N. For sample D (grown prior to sample C) the growth temperature was increased to 460 °C and the nominal N composition was tuned back to the original value used for sample A, due to the excess incorporation of N in structure B, as well as, for accommodating thermally activated increase in the N incorporation with higher T_g [41]. Interestingly, the incorporation of N in sample D was still increased resulting in 1.23 times higher composition compared to the nominal value. Similar behavior was observed for all the samples except for structures C and F. For sample C (grown at 450 °C) the N concentration agreed well with the nominal value. Based on these observations it seems that the incorporation of N is significantly enhanced for these narrow gap materials when the growth temperature exceeds 450 °C (Fig. 1a). Between samples C and D the N composition increases with a slope of 0.023%/°C when normalized with the nominal N composition

Table 2
Bandgap energies, lattice strain and best-fit compositions of the GaInNAsSb layers.

Sample	E_g (eV)	ε_{xx} (%)	[In] (%)	[N] (%)	[Sb] (%)
A	0.83	0.32	15.4	5.3	2.5
B	0.78	−0.12	15.3	6.6	2.6
C	0.84	0.35	15.2	5.2	2.4
D	0.79	0.09	15.2	6.4	2.5
E	0.81	0.25	15.2	6.1	2.3
F[a]	n.a.	n.a.	n.a.	n.a.	n.a.
G	0.80	0.21	15.1	6.2	3.0
H	0.80	0.29	15.1	6.1	3.3
I	0.80	0.39	15.0	6.3	3.2
J	0.80	0.33	14.3	6.2	3.8
K	0.80	0.30	14.1	6.4	3.8

[a] Phase separated material.

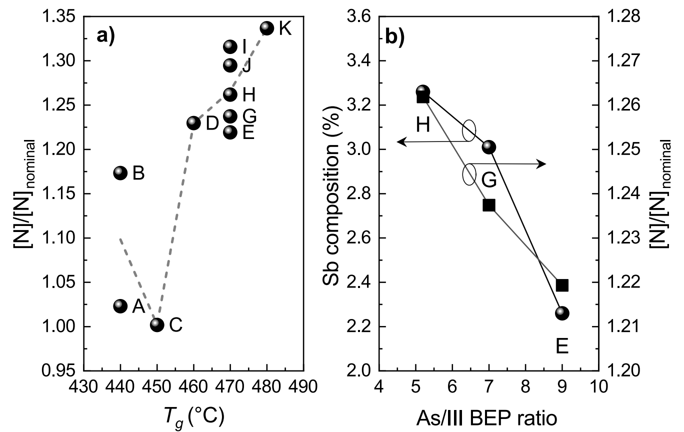

Fig. 1. (a) *The deviation from targeted nitrogen composition as function of the growth temperature. The dashed line represents the average between samples at each T_g as guide for the eye.* **(b)** *The Sb composition and deviation of nominal N composition for samples H, G and E for which the As/III BEP ratio was varied between 5.2 and 9.0.*

of 5.2%, which is approximately ten-fold compared to the composition normalized slope of 0.002%/°C reported for 3% GaInNAs [41]. The large difference between the slope observed here and the slope reported earlier for GaInNAs likely originates from changes in the incorporation kinetics caused by the significantly higher N concentrations and the use of Sb surfactant in this work.

The Sb composition in the T_g sample set was consistently determined to be ~2.5%. But when the As/III BEP ratio was lowered from 9.0 to 5.2 (E, G–H) the Sb composition increased from 2.2% to 3.3% (Fig. 1b). At the same time an increase in the measured N composition can also be seen (Fig. 1b). The higher incorporation of Sb and N with lower As/III BEP ratio is likely to be caused by a reduced competition for the group-V lattice sites by As. When the Sb flux was increased (G, I–J), the Sb composition quite expectedly went linearly from 3.0% to 3.8%.

In terms of crystalline structure, the GaInNAsSb layers were not fully lattice-matched. Majority of the grown GaInNAsSb layers were under slight compressive strain. Slight compressive strain has been found to be beneficial for 1 eV dilute nitride solar cells [42]. Only structure B was determined to be under slight tensile strain, whereas for sample F the strain state could not be reliably determined due to phase separation of the GaInNAsSb material. Despite being strained, all the GaInNAsSb layers except for sample F, showed good coherence with no signs of relaxation in the measured RSMs (Fig. 2a and Fig. 2b). The RSMs measured for sample F quite clearly confirmed the phase separation occurring at the growth temperature of 480 °C and inferior crystalline structure of the GaInNAsSb layer (Fig. 2c and Fig 2d). By employing higher Sb flux (sample K), the phase separation in the high growth temperature regime was inhibited, effectively demonstrating the surfactant effect of Sb reported in literature [43,44].

The PL spectra measured for the samples in the T_g set (A–E, K) did not show any clear dependency on changes in the growth temperature (Fig. 3a). Instead, the PL data shows that the PL emission wavelength of the GaInNAsSb quite expectedly follows the determined N compositions (Fig. 3b). In addition, Fig. 3b shows that the PL signal is reduced when more N is incorporated into the crystal, presumably indicating increased non-radiative recombination in the GaInNAsSb material associated with higher N. Interestingly, the PL signal is not drastically reduced when N goes from 5.2% to 6.1% but drops rapidly when N concentration exceeds 6.1%. The relatively high PL signal measured from structure E (N = 6.1%) could be attributed to more optimal growth conditions, thus suggesting optimal T_g setpoint around 470 °C, close to the limit for phase separation under these experimental conditions, at least in terms of PL signal. The reduction in the As/III BEP ratio (E, G–H) also translates into lower PL signal (Fig. 4). Particularly, when the As/III BEP ratio is

Fig. 2. **(a)** *RSMs measured around symmetric (004) reflection and* **(b)** *asymmetric (-2-24) reflection for sample H witha coherent GaInNAsSb layer.* **(c)** *RSMs measured for sample F around symmetric (004) reflection and* **(d)** *asymmetric (-2-24) reflection, showing phase separation in the GaInNAsSb layer.*

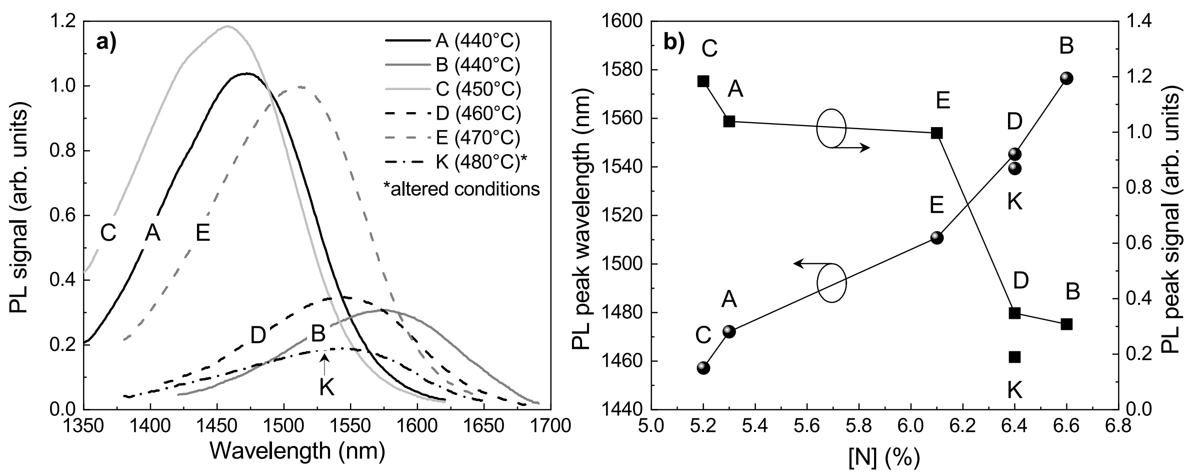

Fig. 3. **(a)** *PL spectra measured using pulsed* 1064 nm *excitation for GaInNAsSb structures grown with varying* T_g. **(b)** *The PL peak signal and wavelength as function of the determined N composition.*

reduced from 9.0 to 7.0 the corresponding PL signal drops by ~70%. In terms of varying the Sb flux (G, I–J), Fig. 4 shows that the PL peak signal first increases by ~36% when the Sb BEP is increased from 1.0×10^{-8} Torr to 1.4×10^{-8} Torr for the growth, showing increase in the luminescent properties of the material. On the other hand, when the Sb BEP is further increased to 1.8×10^{-8} Torr the observed PL peak signal drops close to the original value.

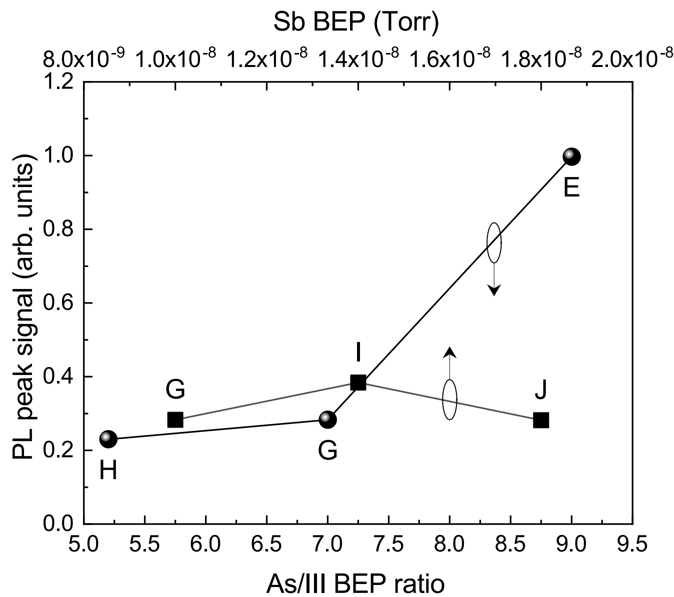

Fig. 4. *Measured PL peak signal as function of As/III BEP ratio (E, G–H) and Sb BEP (G, I–J) used for the growth of the GaInNAsSb layers.*

3.2. Electrical properties

The EQE curves for the experimental GaInNAsSb solar cells measured in 800–1800 nm range along with the measured reflectance of the ARC on n-GaAs substrate are plotted in Fig. 5. Overall, Fig. 5 clearly shows the significant improvement in the EQE values between the initial structures grown at low temperatures (A–B) and the best structure (H) grown with more optimized parameters. With the utilization of better growth conditions, an average increase of 40% for the EQEs between samples B and H was observed. The maximum EQE (EQE_{max}) value rose considerably from 0.69 to 0.94 between samples B and H.

The high EQEs for the GaInNAsSb solar cells in this work are also partially enabled by the low reflectance of the ARC, which has an average reflectance of only 1.2% in the 800–1800 nm wavelength range (Fig. 5). The reflectance spectra measured from a typical sample coated with the same ARC (not shown) were very similar to the ARC on n-GaAs. The reflectance spectra of the coated solar cell materials were used for estimating the internal quantum efficiencies (IQE) of the cells based on the experimental EQE spectra using the relationship IQE = EQE/(1-R), where R is the measured reflectance. Due to the very low reflectance of the coated solar cells, the IQE values show only slight increase compared to the measured EQE values. Nevertheless, the IQE values taken at E_g + 0.2 eV can be used to compare these cells with performance reported earlier [23,45,46]. The IQE values at E_g + 0.2 eV for samples B and H were 0.41 And 0.78, respectively, thus demonstrating significant improvement of the material quality. The IQE for sample H taken at E_g + 0.2 eV surpasses the experimental values of 0.65 and 0.71 reported earlier for 0.78 eV GaInNAsSb cells without back reflector and with back reflector, respectively [35,36]. The value also now exceeds the value of 0.72 demonstrated with a 0.92 eV GaInNAs junction [23].

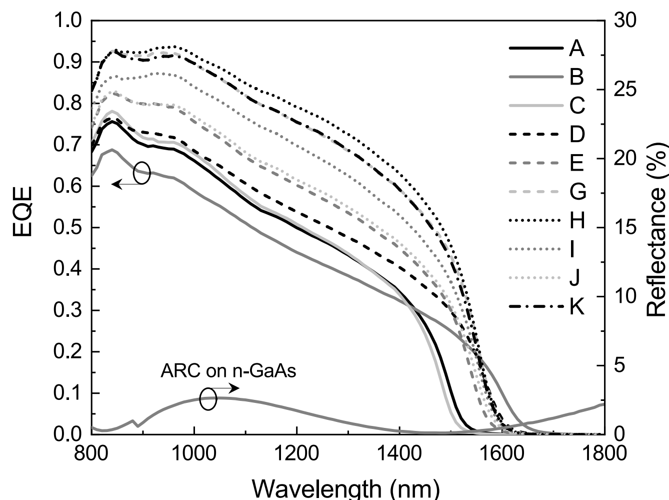

Fig. 5. *EQE spectra measured for the GaInNAsSb structures at wavelengths above 800 nm. Also, the reflectance spectra measured for ARC deposited on n-GaAs substrate is shown.*

The measured EQE spectra were also used for estimating the short-circuit current densities (J_{sc}) for the GaInNAsSb cells at wavelengths above 900 nm using the ASTM G173-03 AM1.5D (1000 W/m^2 normalization) reference spectrum [47]. The significant increase in the EQE between samples B and H translates into the J_{sc} values as the short-circuit current densities for B and H were 10.8 mA/cm^2 and 17.5 mA/cm^2, respectively. The values for peak EQE and IQE at E_g + 0.2 eV along with calculated J_{sc} values are listed in Table 3.

The EQE spectra in Fig. 5 also shows that for all the structures, the EQE decreases at longer wavelengths suggesting transmission losses through the 1200 nm thick GaInNAsSb absorber layers. By employing similar optical modelling method used for analysis of the narrow bandgap back reflector GaInNAsSb cells along with the absorption coefficients reported for 0.8 eV GaInNAsSb [36], the absorbance (A_{DN}) and transmission losses (T_{DN}) in the GaInNAsSb layers could be estimated. Since A_{DN} describes the fraction of incident photons absorbed by the GaInNAsSb, it sets the upper limit for the EQE of the cell. With unity collection efficiency every photon absorbed by the GaInNAsSb material creates charge carriers that are collected by the external circuit, thus causing EQE and A_{DN} to be equal. Recombination losses in the cell reduce the collection efficiency below unity, leading to lower EQE compared to A_{DN}. As seen from Fig. 6, the modelled absorbance for a 1200 nm thick GaInNAsSb layer correlates quite well with the EQE of sample H. The measured EQE is only slightly lower than the modelled A_{DN}, indicating low recombination losses in the junction correlating with a high collection efficiency. In fact, the average collection efficiency in the range of 900–1550 nm for sample H was estimated to be 95%. Since the same GaInNAsSb layer thickness was used for all the structures, then A_{DN} should also be closely similar between the structures. Consequently, as lower EQEs were determined for the other structures compared to the EQE of sample H (Fig. 5), the rest of samples can be analyzed to have lower collection efficiencies because of higher recombination losses in the material.

The optical analysis also shows relatively high transmission losses for the 1200 nm thick GaInNAsSb layers (Fig. 6). In fact, approximately 14% of incident photons of AM1.5D spectrum in the 900–1550 nm range are lost due to incomplete absorption in the GaInNAsSb material. By increasing the effective thickness of the GaInNAsSb layer, either by

Table 3
Determined values for EQE_{max}, values of IQE taken at E_g + 0.2 eV, and calculated J_{sc} values at wavelengths above 900 nm using AM1.5D (1000 W/m^2) reference spectrum.

Sample	EQE_{max}	IQE at E_g + 0.2 eV	J_{sc} (mA/cm^2)
A	0.76	0.51	11.2
B	0.69	0.41	10.8
C	0.78	0.52	11.4
D	0.76	0.51	12.6
E	0.82	0.59	13.7
F	n.a.	n.a.	n.a.
G	0.93	0.74	16.9
H	0.94	0.78	17.5
I	0.87	0.68	15.7
J	0.83	0.60	14.0
K	0.93	0.74	16.9

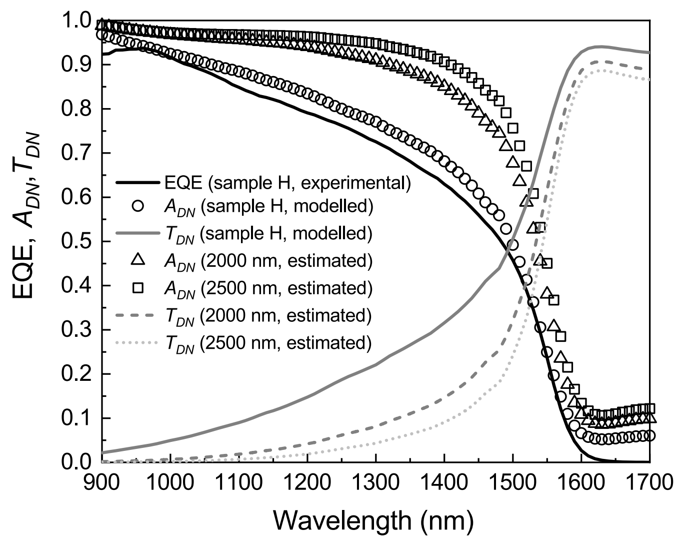

Fig. 6. *Comparison of the EQE and the modelled absorbance of the GaInNAsSb layer for sample H also showing estimated transmission losses. In addition, the improvement in the absorbance and reduction in the transmission losses by employing thicker GaInNAsSb is illustrated with A_{DN} and T_{DN} modelled for 2000 nm and 2500 nm thick GaInNAsSb layers.*

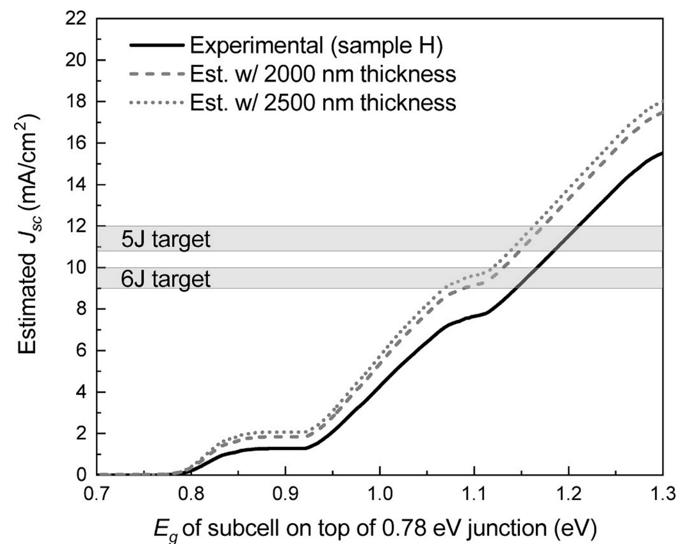

Fig. 7. *Estimated J_{sc} values for the 0.78 eV GaInNAsSb subcell with 1.2 μm (experimental), 2.0 μm (estimated) and 2.5 μm (estimated) absorber thickness under subcells with varying bandgaps. The overlaying subcells are considered to be optically thick, ie. absorbing every photon with energy above E_g. In addition, the J_{sc} targets for 5J and 6J structures are illustrated.*

physically thickening the layers or by employing back reflectors, the absorption could be significantly increased resulting in reduction in the transmission losses. To illustrate this, Fig. 6 includes A_{DN} and T_{DN} estimated for 2000 nm and 2500 nm thick GaInNAsSb layers. The absorbance is significantly increased by employing 2000 nm and 2500 nm thicknesses for the GaInNAsSb layer, and the fraction of photons lost due transmission in the 900–1550 nm would be reduced to 6% and 4%, respectively. By assuming the same collection efficiency for thicker samples as was determined for sample H, the EQE would be significantly enhanced as a result of the increased absorbance. Up to 2.0 mA/cm^2 and 2.6 mA/cm^2 higher J_{sc} values compared to the J_{sc} of 17.5 mA/cm^2 determined for structure H (Table 3) could be expected with 2000 nm and 2500 nm layer thicknesses, respectively. Still, achieving similar collection efficiency might prove to be difficult to realize considering the short carrier diffusion lengths of these materials.

The J_{sc} targets for current-matched 5J and 6J designs would be approximately 10.8–12.0 mA/cm^2 and 9.0–10.0 mA/cm^2, respectively [6,36,48]. If sample H would be used as the bottom junction in a 5J or 6J multijunction cell, beneath an optically thick subcell, these current density targets could be met by employing bandgap energies of ~1.15 eV and ~1.2 eV for the overlying subcell, respectively (Fig. 7). By thinning of the overlaying subcell, therefore allowing a fraction of the photons useable by the upper subcell to be passed to the bottom junction, the E_g of the overlying subcell could be pushed even to lower energies. If the 0.78 eV bottom junction could be fabricated with 2000 nm and 2500 nm absorber thicknesses (as estimated in Fig. 6), current matching could be attained in 5J and 6J designs using optically thick subcells with bandgaps ~1.1 eV and ~1.15 eV, respectively, on top of the bottom junction (Fig. 7). By employing sample H as the bottom junction in the 6J design utilizing a 0.78 eV GaInNAsSb subcell reported earlier [35], the overlying subcell would not require as much thinning, and efficiencies exceeding 52% could be realistically achieved.

The LIV curves for the experimental GaInNAsSb solar cells measured under AM1.5D (1000 W/m^2) with 900 nm high-pass filter are shown in Fig. 8. The experimental J_{sc} values obtained from the LIV measurements follow quite closely the values estimated from the EQE curves shown in Table 3. As expected, sample H with the highest EQE also demonstrated the highest J_{sc} of 17.7 mA/cm^2. A p-type background doping was determined for all the GaInNAsSb samples. Higher current densities are seen for samples with lower background doping densities. This is due to

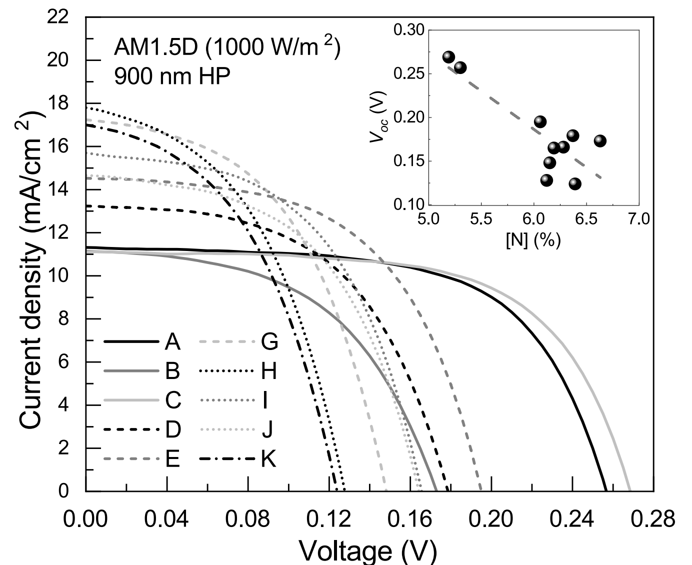

Fig. 8. *The LIV curves measured for the experimental GaInNAsSb structures under 900 nm high-pass filtered AM1.5D (1000 W/m^2) illumination. The inset shows the V_{oc} with respect to the N concentration.*

wider depletion region and thus more efficient collection of the carriers from the dilute nitride layer. A general trend for the LIV curves seen from Fig. 8 is that there is a trade-off between high current generation and high open-circuit voltage (V_{oc}). Clearly higher V_{oc} values were recorded for the cells with the lower N compositions of 5.2–5.3% (A and C), while significantly lower V_{oc} values are determined with N compositions over 6%, which can also be seen from the inset of Fig. 8. The lower V_{oc} values seen with higher N compositions can be partially explained by the reduction of E_g, but it can also be attributed to N related degradation of GaInNAsSb material quality when the N concentration increases. This can also be seen in the simulated carrier lifetimes (τ) shown in Table 4, which show decrease with higher N compositions, thus signaling stronger non-radiative recombination for samples with more N. The N related deterioration of material quality is reflected also

Table 4

LIV characteristics and W_{oc} values determined for the GaInNAsSb with 900 nm high-pass filtered AM1.5D (1000 W/m²) illumination. Dark saturation current densities and ideality factors determined from dark-IV measurements made at 25°C are also shown. In addition, the estimated carrier lifetimes and the p-type background doping densities are included.

Sample	J_{sc} (mA/cm²)	V_{oc} (V)	W_{oc} (V)	FF (%)	J_0 (A/cm²)	n	τ (ns)	Doping density (cm⁻³)
A	11.3	0.26	0.57	63	4.1×10^{-6}	1.33	4.0	1.0×10^{17}
B	11.1	0.17	0.61	52	1.1×10^{-4}	1.67	0.8	3.0×10^{16}
C	11.1	0.27	0.57	63	2.6×10^{-6}	1.31	5.0	1.4×10^{17}
D	13.2	0.18	0.61	54	9.1×10^{-5}	1.55	0.9	1.5×10^{16}
E	14.5	0.20	0.61	56	4.1×10^{-5}	1.40	1.5	1.5×10^{16}
F	n.a.	n.a.	n.a.	n.a.	n.a.	n.a.	n.a.	n.a.
G	17.2	0.15	0.65	50	2.3×10^{-4}	1.50	0.6	2.0×10^{15}
H	17.7	0.13	0.67	47	4.1×10^{-4}	1.50	0.5	1.5×10^{15}
I	15.7	0.17	0.63	53	9.8×10^{-5}	1.39	0.7	5.0×10^{15}
J	14.6	0.17	0.63	53	8.6×10^{-5}	1.36	0.7	7.0×10^{15}
K	17.0	0.12	0.68	46	4.4×10^{-4}	1.52	0.3	1.1×10^{15}

in the dark saturation current densities (J_0) and diode ideality factors (n) listed in Table 4, which were obtained from the dark-IV measurements (Fig. 9) by fitting one-diode model to the experimental data. The J_0 values for the samples with >6% of N are one to two orders of magnitude higher compared to the samples with just over 5% N compositions (A and C), thus signifying increased recombination for samples with higher N. The ideality factors for samples A and C with low N were 1.31 and 1.33, respectively, indicating higher recombination in the quasi-neutral

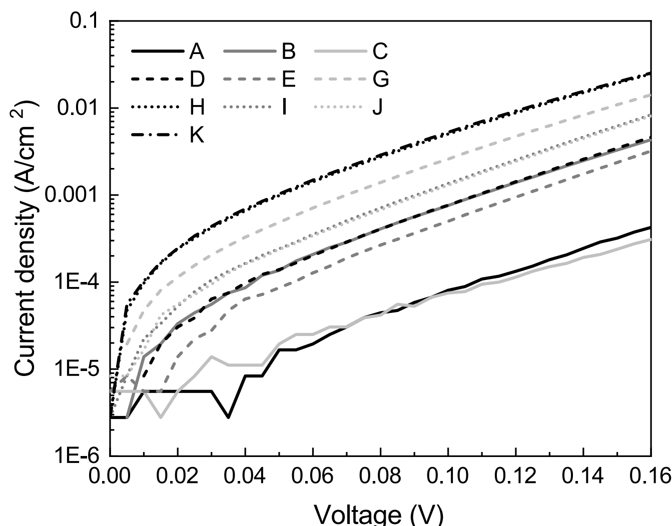

Fig. 9. *Dark-IV curves measured at 25 °C for the experimental GaInNAsSb cells.*

regions. For sample B with the highest N content of 6.6% an ideality factor of 1.67 was determined, signaling higher recombination in the depletion region. The same trend can be observed in the bandgap-voltage offset ($W_{oc} = E_g/q\text{-}V_{oc}$) values of the cells. For samples A and C with lower N compositions the W_{oc} was 0.57 V, which is close to the typical value of 0.55 V for 1 eV dilute nitride solar cells [49,50]. The samples with N over 6% exhibit higher W_{oc} values between 0.61 V and 0.68 V indicating lower material quality. Similar increase in the W_{oc} values close to 0.8 eV bandgap energies was observed previously for narrow bandgap GaInNAsSb solar cells in which only the N content was varied [35], further supporting the claim of N related reduction of V_{oc}. Nevertheless, the W_{oc} values exhibited by these cells are considerably higher than W_{oc} values of approximately 0.3–0.4 V expected for high quality solar cells operating close to the radiative limit [26]. The measured fill factors (FF) also exhibit degradation with increasing N concentration, showing a clear trend corresponding with increase in the J_0 values. The determined LIV characteristics, W_{oc}, J_0 and n values, as well as the simulated carrier lifetimes and background doping densities for the GaInNAsSb cells are shown in Table 4.

3.3. Effects of growth temperature on solar cell performance

The initial growth temperature setpoint of 440 °C for the T_g set (A–F) was chosen based on the optimal growth temperature reported earlier for ~1 eV GaInNAs solar cells [14]. For the subsequent structures it was predicted that the formation of structural defects such as As_{Ga} antisites and Ga vacancies (V_{Ga}), for which the concentration is reported to increase with higher N contents and lower growth temperatures [19,20,51], could be mitigated by using higher T_g. Another motivation for increasing the T_g lies in the background doping of the GaInNAsSb layer. It has been proposed that N-V_{Ga} complexes could act as acceptors in dilute nitrides [52]. Since a p-type background doping was analyzed for 0.8 eV dilute nitride previously [36], it was presumed that by increasing the T_g the concentration of V_{Ga} could be reduced, which should lead to lower background doping density for the GaInNAsSb. Lower background doping densities on the other hand would lead to better depletion of the GaInNAsSb layer, leading to wider depletion region and improved carrier collection. In fact, when the T_g setpoint for the GaInNAsSb is increased from 440 °C towards 480 °C, while keeping the As/III BEP ratio fixed at 9.0 and the Sb BEP at 1.0×10^{-8} Torr, a significant increase in the current generation is observed until 480 °C, at which point the material had undergone phase separation effectively destroying the material and the cell performance. Although sample K is not fully comparable with the samples of the original T_g set (A–F) due to differences in the growth conditions, it shows that by employing higher Sb flux the phase separation at 480 °C was effectively avoided, resulting in further improvement of the J_{sc}. Between samples A and E grown at 440 °C and 470 °C, respectively, the J_{sc} was increased by 28% going from 11.3 mA/cm² to 14.5 mA/cm², whereas sample K grown at 480 °C (with different Sb flux and As/III BEP ratio) exhibited a J_{sc} of 17.0 mA/cm². The evolution of J_{sc} as function of T_g is illustrated in Fig. 10a. The PC1D simulations show that the higher current densities obtained for samples grown at higher T_g can indeed be attributed with better depletion of the GaInNAsSb layer resulting from lower background doping. The level of the p-type background doping is exponentially reduced with higher T_g, which enables wider depletion regions, and thus, improves the collection efficiency for samples grown at elevated growth temperatures. As predicted earlier, the reduction in background doping could be attributed to the reduction of structural defects such as V_{Ga}. Alternatively, the reduction of background doping could be caused by formation of deep non-radiative recombination centers, which could also explain the reduction of minority carrier lifetimes at higher T_g. The higher current densities obtained for samples grown at higher T_g would make it easier to achieve current-matching in a MJSC configuration.

Although one might observe some reduction in the V_{oc} values with higher T_g, the drop in V_{oc} is actually a result of increased dark saturation

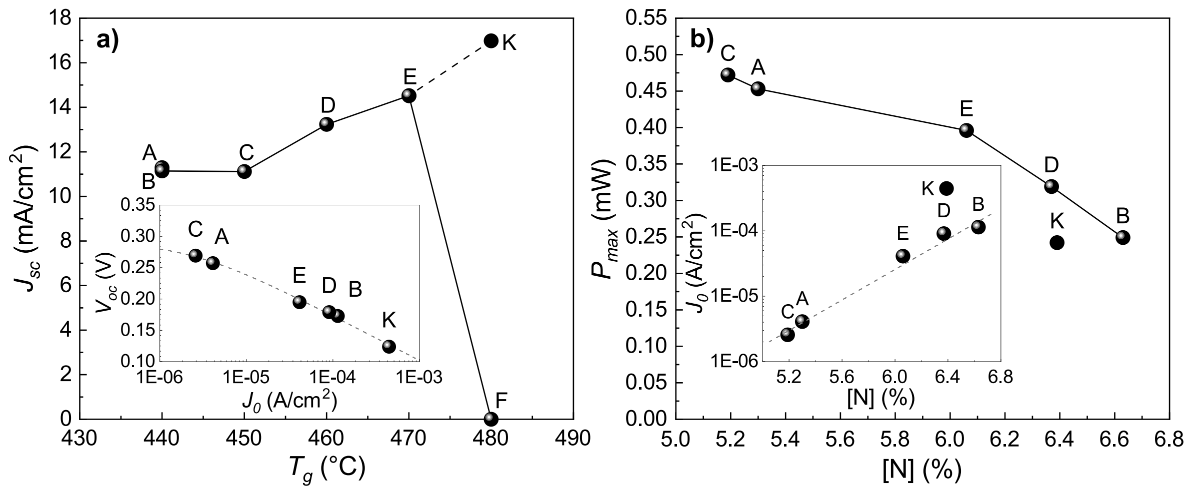

Fig. 10. **a)** *The measured J_{sc} with respect to growth temperature with inset showing the V_{oc} as function of J_0.* **b)** *P_{max} for GaInNAsSb cells grown at different temperatures as function of N concentration with inset illustrating the exponential dependence of J_0 on the N composition.*

current for samples grown at different T_g setpoints (A–E, K) caused by variations in the N compositions between the samples rather than variations in the T_g. This becomes evident from the fact that the measured V_{oc} values are expectedly proportional to the natural logarithm taken from the inverse of J_0 values (Fig. 10a inset), and the J_0 values show exponential dependence on the determined N compositions (Fig. 10b inset). In other words, the differences in the V_{oc} values for the samples with different T_g (A–E, K) is mainly caused by increased recombination resultant from deterioration of the GaInNAsSb material quality with higher N concentrations. The N induced increase in recombination can also be seen in the carrier lifetimes obtained from the simulations (Table 4) as τ is significantly lowered when more N is incorporated into the crystal. Although the reduction in the minority carrier lifetimes also reduces the minority carrier diffusion length, the reduction in the background carrier doping density enables sufficient depletion of the relatively thin 1200 nm GaInNAsSb layer leading to increase in the depletion width of the cells. Therefore, more charge carriers are generated within the depletion region, which increases the field-aided carrier collection of carriers and improves the overall carrier collection even with reduced carrier lifetimes and diffusion lengths. Still, between samples D and E, with identical background doping level of 1.5 $\times$ 10^{16} cm^{-3}, lower J_{sc} is measured for sample D with lower τ, signaling reduced carrier collection due to reduction in the minority carrier diffusion length. The FF values for the cells exhibit a linear dependence with respect to the V_{oc} values. On the other hand, the W_{oc} values show an increase with higher T_g setpoints (Fig. 11), thus still indicating some reduction in material quality with higher T_g.

Consequently, although the J_{sc} increased significantly when higher T_g was used, the maximum power (P_{max}) produced by the cells is more determined by their V_{oc} and FF values, which were deemed more dependent on the N concentration rather than the T_g. In fact, the P_{max} shows decrease as a function of the N concentration (Fig. 10b). So, regardless of samples A and C (with lower N contents) exhibiting lowest J_{sc} values, therefore effectively hampering their use in MJSCs, the highest P_{max} values were recorded for these cells due to their higher V_{oc} and FF values. For structures with >6% N in the T_g set, the highest P_{max} was demonstrated by sample E grown at 470 °C, exhibiting the highest J_{sc} within the set. Despite generating even higher current than sample E, the P_{max} for sample K, grown at 480 °C and slightly modified conditions, was lower due to the lower voltage of the cell.

Based on the experiments, for achieving high current generation enabling current-matching in MJSC architectures, the narrow gap GaInNAsSb materials should be grown close to the high end of the growth temperature range, in this case around 470 °C (i.e. close to the

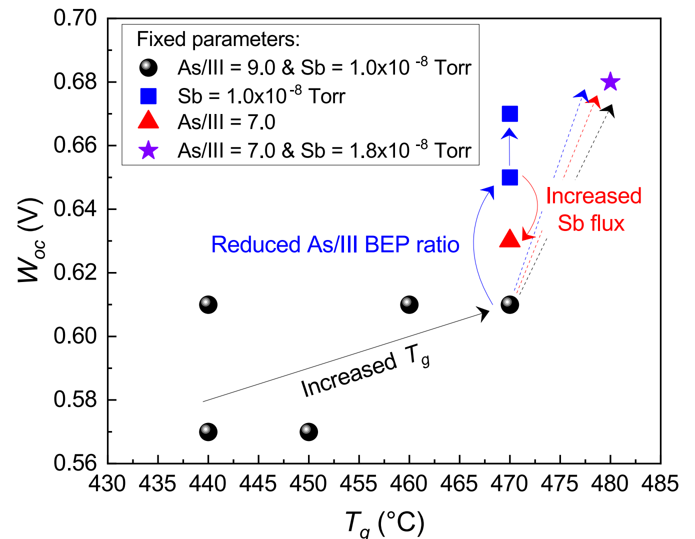

Fig. 11. *W_{oc} values determined for the GaInNAsSb cells as function of growth temperature. Also, the effects of reduced As/III BEP ratio and higher Sb flux on the W_{oc} is shown.*

phase separation limit observed with these growth conditions). On the other hand, the N concentration should be kept as low as possible to reduce the detrimental effects of N incorporation on V_{oc}.

3.4. Effect of As/III BEP ratio on solar cell performance

The As series was based on sample E from the T_g set, which was grown using As/III BEP ratio of 9.0. Samples G and H were grown using lower As/III BEP ratios of 7.0 and 5.2, respectively, while employing the same T_g of 470 °C and Sb BEP of 1.0 $\times$ 10^{-8} Torr used for sample E. Similar to increasing the T_g, lowering the As/III BEP ratio is shown to reduce the concentrations of As_{Ga} antisites and Ga vacancies forming in the dilute nitride [19], therefore potentially reducing the background doping of the material by reducing the concentration of N-V_{Ga} complexes [52]. In fact, a significant reduction in the p-type background doping by using lower As/III BEP ratios for the growth has been previously reported for GaInNAs solar cells [52]. At first glance, this seems to also hold true for the high-N GaInNAsSb as the background doping densities given by the PC1D simulations show reduction when the As/III BEP ratio is reduced for the GaInNAsSb layer. But rather than resulting

from the modification of the defect formation with caused by lower As overpressure, the reduction in the background doping density can be explained with increased Sb surfactant effect when the As/III BEP ratio is reduced. The doping densities seem to correlate with the increase in the Sb composition, which was analyzed to be caused by less competition for the group-V lattice sites when lower As pressures are used (Fig. 12b). This is consistent with the other reports on reduction of background doping with incorporation of Sb [23,53]. The impact of the lower background doping densities can be seen as an increase in the carrier collection as the J_{sc} first increases from 14.5 mA/cm^2 (E) to 17.2 mA/cm^2 (G) and then to 17.7 mA/cm^2 (H), with the As/III BEP ratio going from 9.0 to 7.0 and then to 5.2, respectively (Fig. 12a). In fact, the J_{sc} values demonstrate linear dependence on the determined Sb compositions (Fig. 12a inset). On the other hand, the PC1D simulations indicate that τ increases with larger As/III BEP ratios, signaling decreased recombination and, therefore, improved material quality when more As is used for the growth of the GaInNAsSb. Although the reduction of As/III BEP ratio is seen to reduce the minority carrier lifetime, consequently reducing the minority carrier diffusion length in the GaInNAsSb material, the simultaneous reduction in the p-type background doping close to 1 × 10^{15} cm^{-3} ensures sufficient depletion of the 1.2 μm GaInNAsSb layer, resulting in an increase in the overall carrier collection. Also, the J_0 values show increase in respect with reduction in the As/III BEP ratios (Fig. 12b inset). Consequently, this leads to lower V_{oc} (Fig. 12a) and FF values for GaInNAsSb cells with less As. The reduction in the material quality is also visible in the W_{oc} values, since the W_{oc} increases linearly from 0.62 to 0.67 as the As/III BEP ratio is reduced from 9.0 to 5.2 (see Fig. 11). In terms of power generation, the gain for the J_{sc} obtained by reducing the As/III BEP ratio gets overshadowed by the simultaneous reduction in V_{oc} and FF values, therefore leading to lower $P_{\max}$ values. The $P_{\max}$ reduces linearly from 0.40 mW to 0.26 mW when As/III BEP ratio is lowered from 9.0 to 5.2 (Fig. 12b).

In overall, higher J_{sc} values can be obtained for the narrow gap GaInNAsSb cells by reducing the As pressure for the dilute nitride growth, yet the reduction of As/III BEP ratio lowers the V_{oc} and FF, which consequently reduces the maximum power output of the cell. Similar effects of reducing As/III BEP ratio have been reported earlier for 1 eV GaInNAs solar cells [54]. Nevertheless, sample H exhibits the highest current generation to date for any dilute nitride solar cell with bandgap near 0.8 eV, making a subcell based on this material attractive for integration in a MJSC architecture.

3.5. Effect of Sb flux on solar cell performance

The Sb series was based on sample G from the As-set, grown at 470 °C with As/III BEP ratio of 7.0 and Sb BEP of 1.0 × 10^{-8} Torr. For samples I and J the Sb pressure was increased to 1.4 × 10^{-8} Torr and 1.8 × 10^{-8} Torr, respectively, while keeping the growth temperature and As/III BEP ratio fixed (470 °C and 7.0, respectively). The goal was to study if increase in the Sb flux would improve the material quality and reduce the background doping also for these high-N dilute nitrides. For these samples increase in the Sb flux (and Sb composition) resulted in lower cell currents. The J_{sc} values decreased linearly from 17.2 mA/cm^2 to 14.6 mA/cm^2 when the BEP for Sb was increased from 1.0 × 10^{-8} Torr to 1.8 × 10^{-8} Torr (Fig. 13a), corresponding with the increase in the Sb composition from 3.0% to 3.8% (Table 2). This would suggest that increasing the Sb flux would actually increase the background doping for these samples, therefore reducing the depletion width and consequently carrier collection. In fact, the PC1D simulations for samples G, I and J indicate that the p-type background doping increases with respect to higher Sb composition, going from 2 × 10^{15} cm^{-3} to 7 × 10^{15} cm^{-3} when [Sb] is increased from 3% to 3.8%. Similar increase in the doping density has been analyzed for 1 eV GaInNAsSb when the Sb composition goes above ~2% [55]. On the other hand, increase in the Sb flux has a positive impact on the V_{oc} and FF values. Although higher V_{oc} and FF values are obtained for both samples grown using higher Sb flux (I–J) compared to the base level (G), a local maximum for both parameters can be observed with sample I, grown using Sb BEP of 1.4 × 10^{-8} Torr corresponding to Sb composition of 3.3%. This is illustrated in the inset of Fig. 13a. The increase in the V_{oc} and FF values can mainly be attributed to Sb increasing the GaInNAsSb material quality, since reduction in the J_0 values and increase for the estimated carrier lifetimes is observed for samples with higher Sb flux. This is reflected in the W_{oc} values as they are reduced by 20 mV to 0.63 V when the Sb flux is increased (see Fig. 11). In terms of power generation, the reduction for the J_{sc} is somewhat offset by the improvement of V_{oc} and FF values. In fact, Fig. 13b shows that for the Sb sample set a clear maximum in the $P_{\max}$ values is obtained for sample I, grown using BEP of 1.4 × 10^{-8} Torr for Sb. An increase of 8% is observed in the $P_{\max}$ between samples G and I, grown using BEP of 1.0 × 10^{-8} Torr and 1.4 × 10^{-8} Torr for Sb, respectively.

The Sb sample series shows that by carefully selecting the Sb flux used for growing these narrow gap materials an overall increase in the GaInNAsSb solar cell performance can be obtained owing to improvement in the material quality. Consequently, the adverse effects associated with higher T_g and lower As pressures could be remedied by more

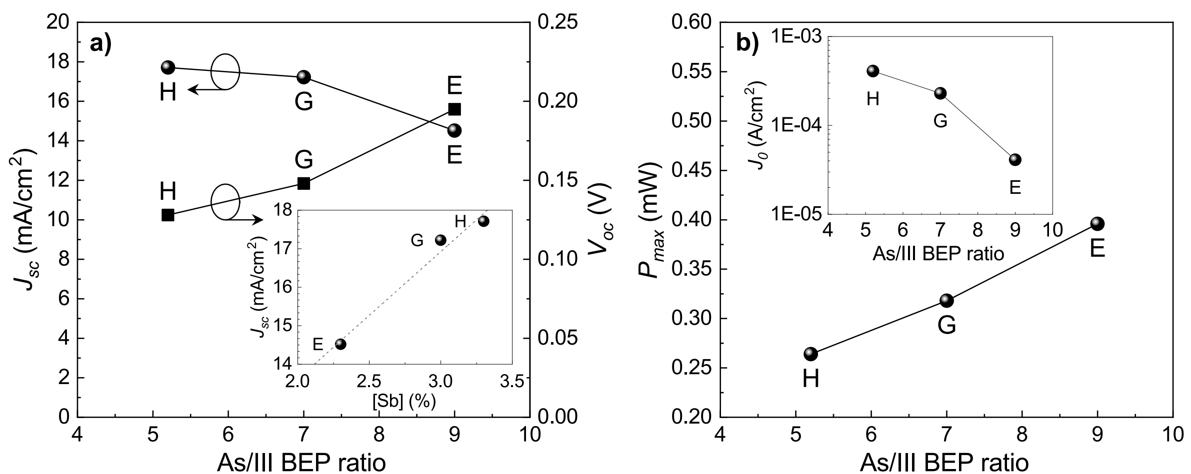

Fig. 12. **a)** *The measured J_{sc} and V_{oc} values with respect to As/III BEP ratio with inset showing the J_{sc} as function of the determined Sb composition.* **b)** *Evolution of $P_{\max}$ as function of As/III BEP ratio with inset illustrating the dependence of J_0 on the As/III BEP ratio.*

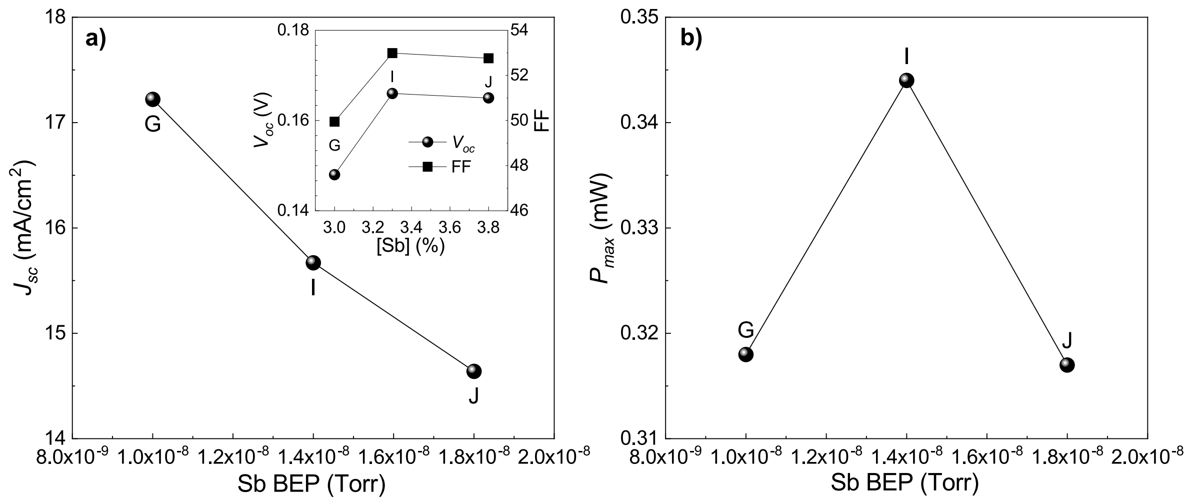

Fig. 13. **a)** *The measured J_{sc} when the Sb BEP is varied. The inset illustrates the V_{oc} and FF values as function of the determined Sb composition.* **b)** *Evolution of $P_{\max}$ with the Sb BEP showing a maximum obtained with the intermediate Sb flux.*

thorough optimization of the Sb fluxes. In addition, sample K demonstrates that by employing higher Sb fluxes the phase separation occurring at higher growth temperatures can be inhibited, effectively increasing the growth parameters range of high-N GaInNAsSb materials.

4. Conclusions

We have studied the effects of growth temperature, As/III BEP ratio, and Sb flux on the performance of high-N GaInNAsSb solar cells lattice-matched to GaAs grown by molecular beam epitaxy. The aim of the investigation was to improve the performance, especially the current generation, of the 0.8 eV GaInNAsSb p-i-n solar cells lattice-matched to GaAs. With that in mind, sets of narrow-bandgap GaInNAsSb p-i-n solar cells with approximately 5–6% nitrogen compositions were grown using growth temperatures of 440–480 °C, As/III BEP ratios of 5.2–9.0 and Sb pressures in the range of 1.0×10^{-8} –1.8×10^{-8} Torr. A significant increase in the EQE and J_{sc} values was seen for the experimental GaInNAsSb cells when these materials were grown at elevated growth temperatures, close to the phase separation, and by lowering the As pressure. The increase in the J_{sc} was attributed to lower p-type background doping in the GaInNAsSb material allowing for better depletion of the *i*-layer and thus enabling better carrier collection. GaInNAsSb cell grown at 470 °C with As/III BEP ratio of 5.2 exhibited a peak EQE of 0.94, IQE at Eg + 0.2 eV of 0.78, generating a J_{sc} of 17.7 mA/cm^2 with AM1.5D (1000 W/m^2) illumination at above 900 nm wavelengths. Our analysis showed that the EQE of this cell is already close to being limited by the absorption in the GaInNAsSb layer. On the other hand, reduction of the material quality was observed with higher T_g and lower As/III BEP ratios, resulting in short carrier lifetimes, higher J_0, and reduced V_{oc}, FF and W_{oc} values. The W_{oc} values for the cells producing the highest currents were 0.65–0.68 V, resulting in low V_{oc} values between 0.12 V and 0.15 V, therefore hindering the efficiency boost gained from the implementation of these subcells in a MJSC structure. In addition, it was seen that the material quality degrades quite rapidly when N concentration goes from 5% to >6%. On the other hand, increasing the Sb flux for the growth of GaInNAsSb improved the material quality, thus yielding in a slight improvement for the V_{oc} and FF, leading to improved power corresponding to a Sb BEP of 1.4×10^{-8} Torr. In addition, it was seen that the phase separation observed at 480 °C could be avoided by employing higher Sb flux, effectively increasing the upper limit for the T_g. Despite the low cell voltages, the improvements obtained for the current generation of the GaInNAsSb subcells in this work would enable fabrication of current-matched MJSC devices using these materials, therefore increasing the viability of these materials for lattice-matched multijunction architectures with 5 or more junctions. Still, we expect that further improvements for the performance of the narrow-bandgap GaInNAsSb junctions would be attained with even more thorough optimization of the growth parameters and annealing.

CRediT authorship contribution statement

Riku Isoaho: Writing – review & editing, Writing – original draft, Visualization, Validation, Resources, Methodology, Investigation, Formal analysis, Conceptualization. **Antti Tukiainen:** Writing – review & editing, Validation, Methodology, Investigation, Formal analysis. **Juuso Puutio:** Writing – review & editing, Resources, Investigation. **Arttu Hietalahti:** Writing – review & editing, Resources, Investigation. **Jarno Reuna:** Writing – review & editing, Resources, Investigation. **Antti Fihlman:** Writing – review & editing, Resources. **Elina Anttola:** Writing – review & editing, Resources. **Miika Keränen:** Writing – review & editing, Visualization, Resources, Investigation. **Arto Aho:** Writing – review & editing, Supervision, Methodology, Conceptualization. **Mircea Guina:** Writing – review & editing, Supervision, Funding acquisition, Conceptualization.

Declaration of competing interest

The authors declare that they have no known competing financial interests or personal relationships that could have appeared to influence the work reported in this paper.

Data availability

Data will be made available on request.

Acknowledgements

The financial support provided by the European Research Council (ERC AdG AMETIST, #695116) is acknowledged. This work is also a part of the Academy of Finland Flagship Program PREIN #320168. In addition, R. I. acknowledges the financial support received from HPY Research Foundation.

References

[1] M.A. Green, E.D. Dunlop, J. Hohl-Ebinger, M. Yoshita, N. Kopidakis, X. Hao, Solar cell efficiency tables (Version 58), Prog. Photovoltaics Res. Appl. 29 (2021) 657–667, https://doi.org/10.1002/PIP.3444.

[2] NREL, Best research-cell efficiency chart (n.d.), https://www.nrel.gov/pv/cell-efficiency.html. (Accessed 22 February 2022).

[3] I.S.E. Fraunhofer, Fraunhofer ISE develops the world's most efficient solar cell with 47.6 percent efficiency. https://www.ise.fraunhofer.de/content/dam/ise/en/documents/press-releases/2022/1322_PR_ISE_World_Record_47,6Percent-SolarCell.pdf, 2022.

[4] M.A. Green, K. Emery, Y. Hishikawa, W. Warta, E.D. Dunlop, Solar cell efficiency tables (version 41), Prog. Photovoltaics Res. Appl. 21 (2013) 1–11, https://doi.org/10.1002/PIP.2352.

[5] V. Sabnis, H. Yuen, M. Wiemer, High-efficiency multijunction solar cells employing dilute nitrides, AIP Conf. Proc. 1477 (2012) 14–19, https://doi.org/10.1063/1.4753823.

[6] A. Aho, R. Isoaho, M. Raappana, T. Aho, E. Anttola, J. Lyytikäinen, A. Hietalahti, V. Polojärvi, A. Tukiainen, J. Reuna, L. Peltomaa, M. Guina, Wide spectral coverage (0.7–2.2 eV) lattice-matched multijunction solar cells based on AlGaInP, AlGaAs and GaInNAsSb materials, Prog. Photovoltaics Res. Appl. (2021) 1–7, https://doi.org/10.1002/pip.3412.

[7] I.S.E. Fraunhofer, Current Status of Concentrator Photovoltaic (CPV) Technology, 2017. https://www.ise.fraunhofer.de/en/publications/studies/studie-current-status-of-concentrator-photovoltaic-cpv-technology.html. (Accessed 17 February 2022).

[8] S.R. Kurtz, D. Myers, J.M. Olson, Projected performance of three- and four-junction devices using GaAs and GaInP, Conf. Rec. IEEE Photovolt. Spec. Conf. (1997) 875–878, https://doi.org/10.1109/PVSC.1997.654226.

[9] C. Himwas, S. Kijamnajsuk, V. Yordsri, C. Thanachayanont, T. Wongpinij, C. Euaruksakul, S. Panyakeow, S. Kanjanachuchai, Optical properties of lattice-matched GaAsPBi multiple quantum wells grown on GaAs (001), Semicond. Sci. Technol. 36 (2021), 045014, https://doi.org/10.1088/1361-6641/ABE65D.

[10] S. Wang, R. Kudrawiec, C. Chia, L. Zhang, X. Zhang, X. Ou, Dilute bismide and nitride alloys for mid-IR optoelectronic devices, Mid-Infrared Optoelectron. Mater. Devices, Appl. (2020) 457–492, https://doi.org/10.1016/B978-0-08-102709-7.00011-5.

[11] I.H. Ho, G.B. Stringfellow, Solubility of nitrogen in binary III–V systems, J. Cryst. Growth 178 (1997) 1–7, https://doi.org/10.1016/S0022-0248(97)00078-X.

[12] D. Schlenker, T. Miyamoto, Z. Chen, M. Kawaguchi, T. Kondo, E. Gouardes, J. Gemmer, C. Gemmer, F. Koyama, K. Iga, Inclusion of strain effect in miscibility gap calculations for III-V semiconductors Japanese J, Appl. Physics, Part 1 Regul. Pap. Short Notes Rev. Pap. 39 (2000) 5751–5757, https://doi.org/10.1143/JJAP.39.5751/XML.

[13] Z. Pan, L.H. Li, W. Zhang, Y.W. Lin, R.H. Wu, Kinetic modeling of N incorporation in GaInNAs growth by plasma-assisted molecular-beam epitaxy, Appl. Phys. Lett. 77 (2000) 214, https://doi.org/10.1063/1.126928.

[14] A. Aho, V. Polojärvi, V.-M. Korpijärvi, J. Salmi, A. Tukiainen, P. Laukkanen, M. Guina, Composition dependent growth dynamics in molecular beam epitaxy of GaInNAs solar cells, Sol. Energy Mater. Sol. Cells 124 (2014) 150–158, https://doi.org/10.1016/j.solmat.2014.01.044.

[15] A. Khan, S.R. Kurtz, S. Prasad, S.W. Johnston, J. Gou, Correlation of nitrogen related traps in InGaAsN with solar cell properties, Appl. Phys. Lett. 90 (2007), 243509, https://doi.org/10.1063/1.2747664.

[16] J.S. Harris Jr., H. Yuen, S. Bank, M. Wistey, V. Lordi, T. Gugov, H. Bae, L. Goddard, in: M. Henini (Ed.), Chapter 1 - MBE Growth and Characterization of Long Wavelength Dilute Nitride III–V Alloys, Elsevier, Amsterdam, 2005, pp. 1–92, https://doi.org/10.1016/B978-008044502-1/50001-9.

[17] W.M. McGee, R.S. Williams, M.J. Ashwin, T.S. Jones, E. Clarke, J. Zhang, S. Tomić, Structure, morphology, and optical properties of Gax In1-x N0.05 As0.95 quantum wells:Influence of the growth mechanism, Phys. Rev. B Condens. Matter 76 (2007), 085309, https://doi.org/10.1103/PHYSREVB.76.085309/FIGURES/7/MEDIUM.

[18] X. Kong, A. Trampert, E. Tournı́, K.H. Ploog, Decomposition in as-grown (Ga,In)(N,As) quantum wells, Appl. Phys. Lett. 87 (2005), 171901, https://doi.org/10.1063/1.2108108.

[19] W.M. Chen, I.A. Buyanova, C.W. Tu, Defects in dilute nitrides: significance and experimental signatures, IEE Proc. - Optoelectron. 151 (2004) 379–384, https://doi.org/10.1049/IP-OPT:20040939.

[20] T. Ahlgren, E. Vainonen-Ahlgren, J. Likonen, W. Li, M. Pessa, Concentration of interstitial and substitutional nitrogen in GaNxAs1−x, Appl. Phys. Lett. 80 (2002) 2314, https://doi.org/10.1063/1.1465522.

[21] D.J. Friedman, A.J. Ptak, S.R. Kurtz, J.F. Geisz, Analysis of depletion-region collection in GaInNAs solar cells, in: Conf. Rec. Thirty-First IEEE Photovolt. Spec. Conf. 2005, 2005, pp. 691–694, https://doi.org/10.1109/PVSC.2005.1488225.

[22] I.A. Buyanova, W.M. Chen, C.W. Tu, Recombination processes in N-containing III–V ternary alloys, Solid State Electron. 47 (2003) 467–475, https://doi.org/10.1016/S0038-1101(02)00390-8.

[23] D.B. Jackrel, S.R. Bank, H.B. Yuen, M.A. Wistey, J.S. Harris, A.J. Ptak, S. W. Johnston, D.J. Friedman, S.R. Kurtz, Dilute nitride GaInNAs and GaInNAsSb solar cells by molecular beam epitaxy, J. Appl. Phys. 101 (2007), 114916, https://doi.org/10.1063/1.2744490.

[24] R. Campesato, A. Tukiainen, A. Aho, G. Gori, R. Isoaho, E. Greco, M. Guina, 31% European InGaP/GaAs/InGaAs solar cells for space application, E3S Web Conf 16 (2017) 3003, https://doi.org/10.1051/e3sconf/20171603003.

[25] A. Aho, R. Isoaho, A. Tukiainen, V. Polojärvi, M. Raappana, T. Aho, M. Guina, Performace of dilute nitride triple junction space solar cell grown by MBE, E3S Web Conf. 16 (2017) 3008, https://doi.org/10.1051/e3sconf/20171603008.

[26] R.R. King, D. Bhusari, A. Boca, D. Larrabee, X.Q. Liu, W. Hong, C.M. Fetzer, D. C. Law, N.H. Karam, Band gap-voltage offset and energy production in next-generation multijunction solar cells, Prog. Photovoltaics Res. Appl. 19 (2010) 797–812, https://doi.org/10.1002/pip.1044.

[27] A. Luque, Will we exceed 50% efficiency in photovoltaics? J. Appl. Phys. 110 (2011), 31301 https://doi.org/10.1063/1.3600702.

[28] S.P. Bremner, C. Yi, I. Almansouri, A. Ho-Baillie, M.A. Green, Optimum band gap combinations to make best use of new photovoltaic materials, Sol. Energy 135 (2016) 750–757, https://doi.org/10.1016/J.SOLENER.2016.06.042.

[29] A. Aho, A. Tukiainen, V. Polojärvi, V. Korpijärvi, A. Gubanov, J. Salmi, M. Guina, P. Laukkanen, Lattice matched dilute nitride materials for III-V high-efficiency multi-junction solar cells: growth parameter optimization in molecular beam epitaxy, 26th Eur. Photovolt. Sol. Energy Conf. Exhib. (2011) 58–61, https://doi.org/10.4229/26THEUPVSEC2011-1AO.8.3.

[30] M.A. Wistey, S.R. Bank, H.B. Yuen, H. Bae, J.S. Harris, Nitrogen plasma optimization for high-quality dilute nitrides, J. Cryst. Growth 278 (2005) 229–233, https://doi.org/10.1016/J.JCRYSGRO.2004.12.060.

[31] X. Yang, M.J. Jurkovic, J.B. Heroux, W.I. Wang, Molecular beam epitaxial growth of InGaAsN:Sb/GaAs quantum wells for long-wavelength semiconductor lasers, Appl. Phys. Lett. 75 (1999) 178–180, https://doi.org/10.1063/1.124311.

[32] A.J. Ptak, R. France, C.-S. Jiang, R.C. Reedy, Effects of bismuth on wide-depletion-width GaInNAs solar cells, J. Vac. Sci. Technol. B Microelectron. Nanom. Struct. Process. Meas. Phenom. 26 (2008) 1053, https://doi.org/10.1116/1.2837848.

[33] H.B. Yuen, Growth and Characterization of Dilute Nitride Antimonides for Long-Wavelength Optoelectronics - NASA/ADS, Stanford University, 2006.

[34] J. Pakarinen, C.S. Peng, J. Puustinen, P. Laukkanen, V.M. Korpijärvi, A. Tukiainen, M. Pessa, Postgrowth annealing of GaInAs/GaAs and GaInAsN/GaAs quantum well samples placed in a proximity GaAs box: a simple method to improve the crystalline quality, Appl. Phys. Lett. 92 (2008), 232105, https://doi.org/10.1063/1.2943157.

[35] R. Isoaho, A. Aho, A. Tukiainen, T. Aho, M. Raappana, T. Salminen, J. Reuna, M. Guina, Photovoltaic properties of low-bandgap (0.7–0.9 eV) lattice-matched GaInNAsSb solar junctions grown by molecular beam epitaxy on GaAs, Sol. Energy Mater. Sol. Cells 195 (2019) 198–203, https://doi.org/10.1016/j.solmat.2019.02.030.

[36] R. Isoaho, T. Aho, A. Aho, A. Tukiainen, J. Reuna, M. Raappana, M. Guina, High performance low-bandgap (0.8 eV) single junction GaInNAsSb solar cells incorporating Au-based back surface reflectors, Sol. Energy Mater. Sol. Cells 234 (2022), 111413, https://doi.org/10.1016/J.SOLMAT.2021.111413.

[37] A. Aho, V.-M. Korpijärvi, A. Tukiainen, J. Puustinen, M. Guina, Incorporation model of N into GaInNAs alloys grown by radio-frequency plasma-assisted molecular beam epitaxy, J. Appl. Phys. 116 (2014), https://doi.org/10.1063/1.4903318.

[38] R. Isoaho, A. Aho, A. Tukiainen, T. Salminen, M. Guina, Bandgap energy model for GaInNAsSb/GaAs alloys with high N content and strain influence, J. Cryst. Growth 584 (2022), 126574, https://doi.org/10.1016/J.JCRYSGRO.2022.126574.

[39] D.A. Clugston, P.A. Basore, PC1D version 5: 32-bit solar cell modeling on personal computers, in: Conf. Rec. Twenty Sixth IEEE Photovolt. Spec. Conf. - 1997, 1997, pp. 207–210, https://doi.org/10.1109/PVSC.1997.654065.

[40] M. Gladysiewicz, R. Kudrawiec, M.S. Wartak, Theoretical studies of optical gain tuning by hydrostatic pressure in GaInNAs/GaAs quantum wells, J. Appl. Phys. 115 (2014), 33515, https://doi.org/10.1063/1.4862230.

[41] V.M. Korpijärvi, A. Aho, P. Laukkanen, A. Tukiainen, A. Laakso, M. Tuominen, M. Guina, Study of nitrogen incorporation into GaInNAs: the role of growth temperature in molecular beam epitaxy, J. Appl. Phys. 112 (2012), 023504, https://doi.org/10.1063/1.4737127.

[42] R.E. Jones-Albertus, H.B. Yuen, T. Liu, P. Misra, US20110232730A1 - Lattice Matchable Alloy for Solar Cells, 2011.

[43] S.R. Bank, H. Bae, L.L. Goddard, H.B. Yuen, M.A. Wistey, R. Kudrawiec, J.S. Harris, Recent Progress on 1.55-μm dilute-nitride lasers, IEEE J. Quant. Electron. 43 (2007) 773–785, https://doi.org/10.1109/JQE.2007.902301.

[44] H.B. Yuen, S.R. Bank, H. Bae, M.A. Wistey, J.S. Harris, The role of antimony on properties of widely varying GaInNAsSb compositions, J. Appl. Phys. 99 (2006), 093504, https://doi.org/10.1063/1.2191745.

[45] A.J. Ptak, D.J. Friedman, S. Kurtz, J. Kiehl, Enhanced-depletion-width GaInNAs solar cells grown by molecular-beam epitaxy, Conf. Rec. IEEE Photovolt. Spec. Conf. (2005) 603–606, https://doi.org/10.1109/PVSC.2005.1488203.

[46] S.L. Tan, W.M. Soong, M.J. Steer, S. Zhang, J.S. Ng, J.P.R. David, Dilute nitride GaInNAs and GaInNAsSb for solar cell applications, Proc. SPIE 8256, Physics, Simulation, Photonic Eng. Photovolt. Devices (2012) 82561E, https://doi.org/10.1117/12.910349.

[47] ASTM G173-03: Standard Tables for Reference Solar Spectral Irradiances: Direct Normal and Hemispherical on 37° Tilted Surface, ASTM International, West Conshohocken, PA, 2003.

[48] J.F. Geisz, R.M. France, K.L. Schulte, M.A. Steiner, A.G. Norman, H.L. Guthrey, M. R. Young, T. Song, T. Moriarty, Six-junction III–V solar cells with 47.1% conversion efficiency under 143 Suns concentration, Nat. Energy 5 (2020) 326–335, https://doi.org/10.1038/s41560-020-0598-5.

[49] N. Leong, K.H. Tan, W.K. Loke, S. Wicaksono, D. Li, S.F. Yoon, P. Sharma, T. Milakovich, M. Bulsara, G. Fitzgerald, Growth of 1-eV GaNAsSb-based photovoltaic cell on silicon substrate at different As/Ga beam equivalent pressure ratios, Prog. Photovoltaics Res. Appl. 24 (2016) 340–347, https://doi.org/10.1002/pip.2705.

[50] A. Aho, A. Tukiainen, V. Polojärvi, J. Salmi, M. Guina, High Current Generation in Dilute Nitride Solar Cells Grown by Molecular Beam Epitaxy, SPIE, 2013, p. 86201I, https://doi.org/10.1117/12.2002972.
[51] J. Slotte, K. Saarinen, E.M. Pavelescu, T. Hakkarainen, M. Pessa, Nitrogen related vacancies in GaAs based quantum well superlattices, Appl. Phys. Lett. 89 (2006), 061903, https://doi.org/10.1063/1.2335402.
[52] V. Polojärvi, A. Aho, A. Tukiainen, M. Raappana, T. Aho, A. Schramm, M. Guina, Influence of As/group-III flux ratio on defects formation and photovoltaic performance of GaInNAs solar cells, Sol. Energy Mater. Sol. Cells 149 (2016) 213–220, https://doi.org/10.1016/J.SOLMAT.2016.01.024.
[53] A.J. Ptak, D.J. Friedman, S. Kurtz, Effects of temperature, nitrogen ions, and antimony on wide depletion width GaInNAs, J. Vac. Sci. Technol. B Microelectron. Nanom. Struct. Process. Meas. Phenom. 25 (2007) 955, https://doi.org/10.1116/1.2715993.
[54] F. Langer, S. Perl, S. Höfling, M. Kamp, p- to n-type conductivity transition in 1.0 eV GaInNAs solar cells controlled by the V/III ratio, Appl. Phys. Lett. 106 (2015), 063905, https://doi.org/10.1063/1.4909507.
[55] A. Aho, Dilute Nitride Multijunction Solar Cells Grown by Molecular Beam Epitaxy, Tampere University of Technology, 2015.